Forecasting and Seismic Detection of Proglacial Debris Flows at Mount Rainier National Park, Washington, USA

SCOTT R. BEASON*

Mount Rainier National Park, U.S. National Park Service, 55210 238th Avenue E, Ashford, WA 98304

NICHOLAS T. LEGG

Wolf Water Resources, 1001 SE Water Avenue, Suite 180, Portland, OR 97214

TAYLOR R. KENYON
ROBERT P. JOST

Mount Rainier National Park, U.S. National Park Service, 55210 238th Avenue E, Ashford, WA 98304

Key Terms: *Debris Flows, Glacial Outburst Floods, Hazard Mitigation and Monitoring, Hazard Forecasting, Real-Time Seismic Amplitude Measurement, Mount Rainier*

ABSTRACT

The glaciated Mount Rainier volcano in southwestern Washington State (United States) has a rich history of outburst floods and debris flows that have adversely impacted infrastructure at Mount Rainier National Park in the 20th and 21st centuries. Retreating glaciers leave behind vast amounts of unconsolidated till that is easily mobilized during high-precipitation-intensity storms in the fall months, and during outburst floods during warm summer months. Over 60 debris flows and outburst floods have been documented between 1926 and 2019 at Mount Rainier. Debris-flow activity has led to the closure of campgrounds and visitor destinations, which has limited visitor access to large swaths of the park. This paper documents efforts to characterize and seismically monitor debris flows, map hazards, and develop forecasting approaches for wet and dry weather debris flows. Using the day-of and historic antecedent weather conditions on past debris-flow days, we developed a debris-flow hazard model to help predict those days with a higher relative hazard for debris-flow activity park-wide based on prevailing and forecasted weather conditions. Debris flows are detected in near-real-time using the U.S. Geological Survey Real-time Seismic Amplitude Measurement (RSAM) tool. If an event is detected, we can then provide evacuation alerts to employees and visitors working and recreating in the areas downstream. Our goal is to accurately forecast the debris-flow hazards up to 7 days ahead of time and then use RSAM to detect debris flows within minutes of their genesis.

INTRODUCTION

Mount Rainier (MORA) is a 4,392 m (14,410 ft) stratovolcano located in southwest Washington State, United States, approximately 70 km (43 mi) southeast of Tacoma and 90 km (56 mi) south-southeast of Seattle (Figure 1). The volcano occupies most of the 956 km^2 (369 mi^2) Mount Rainier National Park and is visible from much of western Washington State. MORA has been episodically active in the last 500,000 years, including at least 10 to 12 eruptions in the last 2,600 years (Sisson and Vallance, 2009). Eruptions have initiated large lahars that have inundated areas of the Puget Lowland as far as 100 km (62 mi) from the volcano (Crandell, 1971). Because of its far-reaching lahar hazards, MORA has a "very high" threat and ranks as the third most hazardous volcano in the nation (Ewert et al., 2018). In addition to these far-reaching hazards, local-scale debris flows induced by hydrologic and surficial geomorphic processes represent a significant management concern on a more frequent and local basis within MORA park boundaries.

Debris flows initiated during intra-eruptive periods at MORA are generally much smaller in magnitude and impact than the large lahars that have occurred during eruptive periods (Pierson and Scott, 1985; Vallance and Scott, 1997; and Vallance, 2005). This type of debris flow is initiated when surges of water

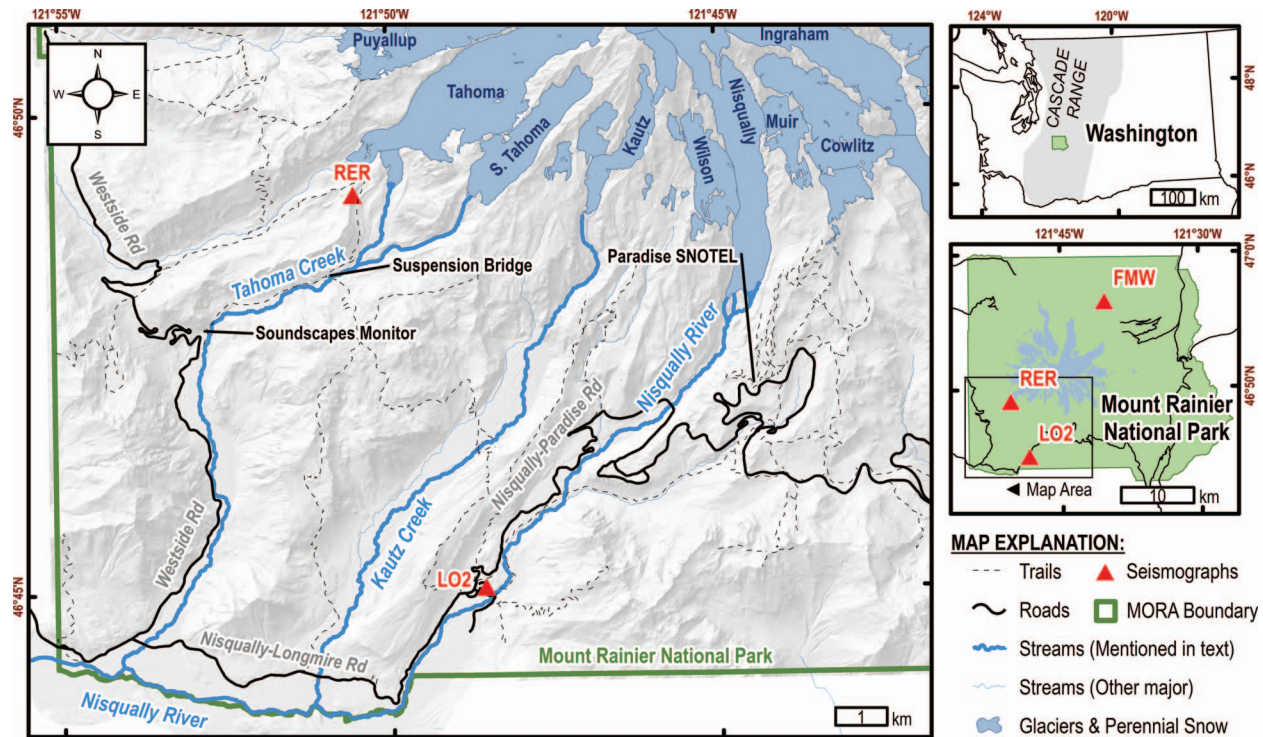*Corresponding author email: scott_beason@nps.gov

Figure 1. Location map of the southwest side of Mount Rainier National Park in Washington State, United States. RER, LO2, and FMW refer to the Emerald Ridge, Longmire, and Mt. Fremont seismographs, respectively. Locations mentioned in text are shown on the detail map.

recruit available loose sediment and transform into rheologically denser slurries of sediment capable of moving large grain sizes (Scott et al., 1995). These surges originate from within a glacier, referred to as glacial outburst floods, or during periods of intense and prolonged precipitation. Debris flows of this type attenuate rapidly, and the deposits are often reworked by subsequent event runoff, leaving them nearly identical to overbank flood deposits. Sometimes, these debris flows often go unnoticed in remote reaches of the park. Understanding the initiation characteristics and thus cataloging all events at MORA are the prime motivating factors in the development of the real-time detection efforts, which was one of the main objectives of this study.

The glaciers in MORA are one of the strongest controlling influences on the park landscape (Lescinsky and Sisson, 1998). MORA has 29 named glaciers, which cover a total of 78.76 ± 1.11 km^2 (30.41 ± 0.43 mi^2) and encompass a total volume of 3.22 ± 0.31 km^3 (0.77 ± 0.07 mi^3) as of 2015 (Beason, 2017; George and Beason, 2017). Studies show that the glacial ice on MORA has decreased in area by 39.1 percent from 1896 to 2015 (0.44 km^2 yr^{-1} avg.) and in volume by 45 percent from 1896 to 2015 (0.02 km^3 yr^{-1}) (Driedger and Kennard, 1986; George and Beason, 2017). Glacial recession contributes to increases in

glacial melt runoff and, through mechanisms not yet understood, subglacial water storage, both of which have been observed to cause glacial outburst floods and many of the debris flows recorded in the park (Walder and Driedger, 1994a, 1994b, 1995). As such, quantification of the changes in these glaciers and the impacts of newly uncovered glacial sediment stockpiles must be considered if we are to understand the hazards discussed here.

This paper documents concerted efforts by the MORA park geologists and a broader research community to monitor debris flows, assess and map hazards, and forecast debris flows to minimize risks to people and infrastructure.

BRIEF HISTORY OF DEBRIS FLOWS AT MOUNT RAINIER

Notable and well-documented debris flows in the park provide a reference point for the processes, initiation mechanisms, and impact of these events, helping to set the stage for the more technical study to follow. The first recorded debris flow in the park occurred in the Nisqually River watershed (Figure 1), on the south side of the park, on October 16, 1926. This event was initiated by the first heavy rain at the end of the summer season (Richardson, 1968). Prior to the event, it

was noted that there was 33 cm (13 in.) of snow at Paradise on October 13, all of which had melted by October 16. After this melt, a warm rain event brought in 9.9 cm (3.9 in.) of rain on the day of the 16th. Between 1932 and 1976, at least six additional outburst floods or debris flows occurred in the Nisqually River, originating from the Nisqually Glacier. Most of these events were induced by precipitation, which varied from 6 to 25 cm (2.4 to 9.9 in.). Four of the events occurred in October, and two occurred in June and July. On October 14, 1932, visiting engineers from the Bureau of Public Lands witnessed a precipitation-induced debris flow, described as "a wall of water 25 ft high and 125 ft wide" and "similar to a huge mixture of concrete except darker in color" (Richardson, 1968). The force of this event moved the entire old Nisqually Glacier Bridge over 0.8 km (0.5 mi) downstream from its original location. Some of the debris-flow events were well documented, including the October 25, 1955, and July 3, 1976, events (Richardson, 1968; Samora and Malver, 1996). An event in 1955 had six pulses in 45 minutes, an estimated velocity of 6.1 m s^{-1}, and a discharge of 2,000 m^3 s^{-1}, and it was estimated to be 70 percent sediment by volume (Richardson, 1968). This event also led to the construction of the current Nisqually Glacier Bridge, a tall, channel-spanning structure that exists to this day.

There are an additional five events cataloged in the Nisqually watershed during the park's history, which behaved similarly to the events listed but were much smaller and had negligible impacts on park infrastructure. These five data points contain three glacial outbursts and two "other hydrologic events." Two of the outburst floods are wet events that were preceded by notably intense rainfall in a short period beforehand, with the other being a dry weather event that took place in July. Of these, only the dry weather event was noted to have multiple surges. The "other hydrologic events" were noted for increases in stream stage, but these were not significant enough to cause any lasting damage to infrastructure or mobilize mass-wasting events. The most recent event recorded in the Nisqually River was a precipitation-initiated outburst flood on October 27, 2012 (Beason, 2012), which caused a 1 m (3 ft) increase in river stage at Longmire, approximately 7.9 km (4.9 mi) downstream of the glacier.

1947 Kautz Mudflow

The largest recorded debris-flow event in the history of MORA is the 1947 Kautz Mudflow, which had an estimated volume of 3.8 × 10^7 m^3. In the 24 hours prior to the event, 15 cm (5.9 in.) of heavy rain and high freezing levels were seen in the Kautz Creek watershed on the south-southwest side of the peak (Figure 1) (Driedger and Fountain, 1989). These conditions resulted in the collapse of the lower 1.6 km (1 mi) of the Kautz Glacier and a rapid release of water stored within the glacier (Scott et al., 1995). The surge of water entrained glacial outwash material, transforming into a clay-poor debris flow (Scott et al., 1995). Deposition of the Kautz Mudflow occurred over several days and included multiple pulses of water. Debris flows were noted in other drainages during this event, including in the Nisqually River.

South Tahoma Glacier Activity

Tahoma Creek and the South Tahoma Glacier, on the southwest side of the peak (Figure 1), have been a notable locus of debris-flow activity in the last half century, which largely began during the summer of 1967. The summer of 1967 was noted as exceptionally warm and dry. On August 29, a short-lived outburst flood destroyed a footbridge 1.9 km (1.2 mi) below the South Tahoma Glacier. The stream rose about 0.5 m (1.5 ft) at the Tahoma Creek Campground, approximately 5.6 km (3.5 mi) downstream of the glacier. Two days later, an outburst flood swept down Tahoma Creek (Richardson, 1968). Fortunately, the campground was already closed due to fire weather danger.

Between 1967 and 2019, at least 33 distinct debris-flow events have originated from the South Tahoma Glacier and flowed down Tahoma Creek (Figure 2). Walder and Driedger (1994a) noted that the record for debris flows in Tahoma Creek does have some gaps, specifically between 1967 and 1985. This is due to poor record-keeping during this time. Crandell (1971, p. 60) noted that, "Floods not associated with rainfall also moved down the [Tahoma Creek] valley from time to time during the summer of 1968." Walder and Driedger (1994a) noted that debris flows from the years of 1971 to 1985 are described "only sketchily" in park records. Debris flows that occurred between 1986 and 1992 are well documented, largely owing to increased awareness among National Park Service staff (Walder and Driedger, 1994a).

The cumulative impact of over 30 debris flows in less than half a century and a major flood event in 2006 (Bullock et al., 2007) has had remarkable impacts to human infrastructure in the Tahoma Creek valley. The 24 km (15 mi) Westside Road was closed to vehicular traffic at mile post 3 in 1988. The sudden increase in debris-flow deposition forced the westward lateral migration and avulsion of Tahoma Creek, completely decimating an old-growth forest in the process (Figure 3). Portions of the Westside Road in Figure 3 have had to be repaired numerous times due to the combined ef-
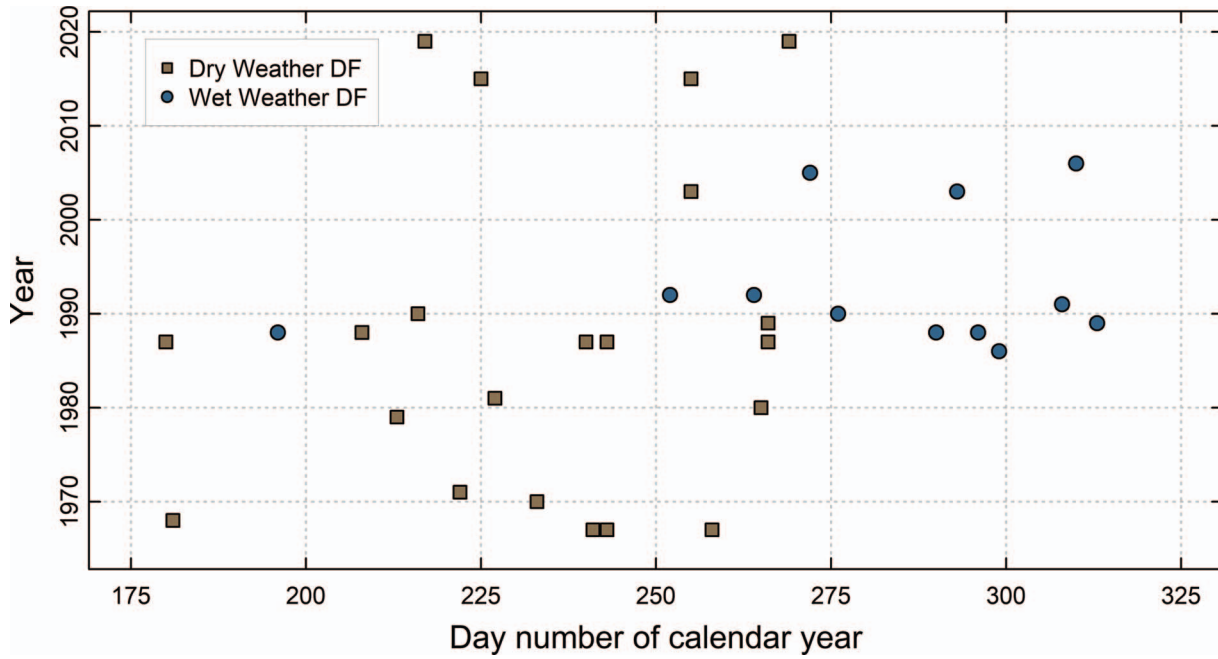
Figure 2. Seasonal timing of debris flows in Tahoma Creek from 1967 to 2019. Dry weather debris flows refer to those initiated by glacial outburst floods generally in the summer season, whereas wet weather debris flows generally occur in the fall and winter and are associated with intense precipitation.
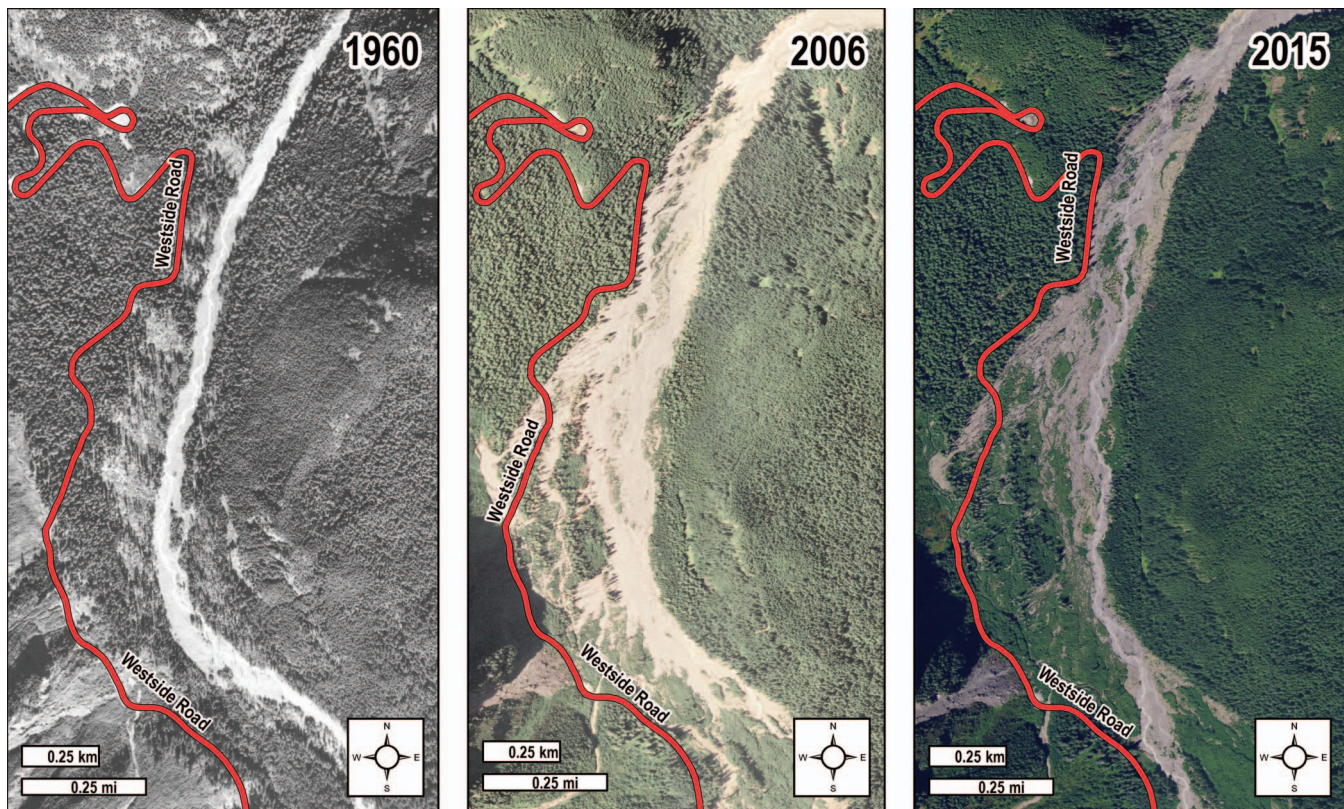

Figure 3. Aerial photos from 1960, 2006, and 2015 showing the westward lateral migration of Tahoma Creek along the Westside Road due to debris-flow activity (related to fan deposition).
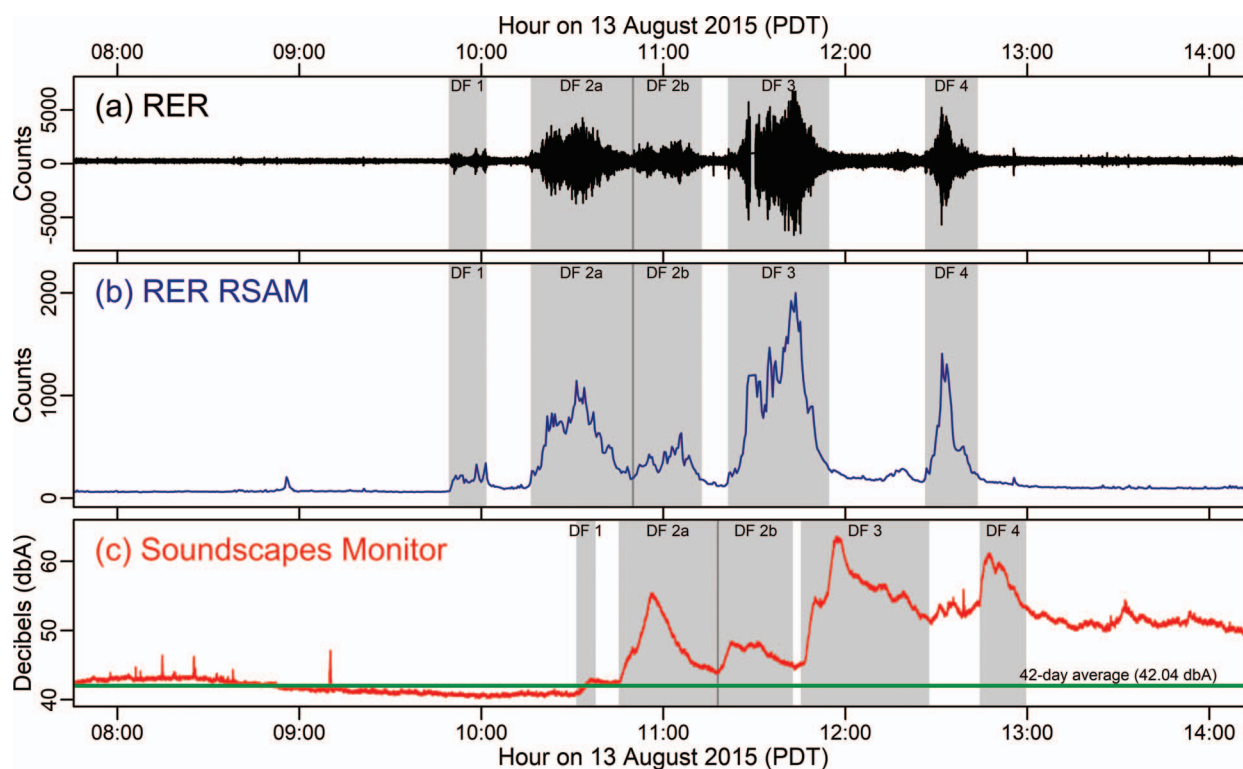
Figure 4. Comparison of waveforms from (a) Emerald Ridge seismograph (RER), (b) real-time seismic amplitude measurement of the Emerald Ridge seismograph (RER RSAM), and (c) Tahoma Creek soundscape monitor during the August 13, 2015, debris-flow sequence. RER and RER RSAM were computed at the same geographic location, whereas the soundscapes monitor was approximately 3.7 km (2.3 mi) downstream, which accounts for the lag in arrival times for that instrument. The green line in plot (c) is the 42 day background average of 42.04 dBA (dBA is based on the intensity of sound and how the human ear responds to that sound). Individual debris-flow pulses are shown in the charts by the vertical gray columns and are numerically labeled as "DF X" based on their order in the sequence.

fects of debris flows and seasonal floods. The reduction in vehicular traffic and thus foot traffic on the Westside Road has led to a rapid and dramatic decrease in the recreational use of the trails and campgrounds on this side of the park since the late 1980s.

Debris Flows in 2015—Direct Observations and Monitoring Results

After a lull in debris-flow activity in the Tahoma Creek basin between 2006 and 2015, four separate debris-flow sequences occurred between 09:49 AM and 12:44 PM PDT (16:49–19:44 UTC) on August 13, 2015, during the park's dry summer season. This event is the best-documented debris flow in the park's history due to a network of flow, sound, and seismic instruments, which recorded the event, as well as direct witness observation of debris-flow pulses. Each individual sequence was identified in seismic records from the Emerald Ridge (RER) seismograph, located near Tahoma Creek (Figure 4; see location in Figure 1). Seismic monitors, a soundscape monitor, and stream gauges downstream all recorded data relevant to each

debris-flow surge, while numerous park visitors, volunteers, and employees all witnessed and photographed the event. Several visitors, including a geology professor at Pacific Lutheran University, recorded photos and videos of individual flows. A park volunteer in the upper Tahoma Creek basin accurately recorded and documented hyperconcentrated flow surges (not recorded on the seismograph) after the four debris flows, recording a total of 12 individual hyperconcentrated flows.

The first debris flow issued by the South Tahoma Glacier was witnessed by visitor Croil Anderson. Anderson described the event as being "louder than a jet" at a distance of 2.5 km (1.5 mi) from the glacier (Anderson, 2015, personal communication). Anderson also stated that the first debris flow was an "incredibly large surge of black water, ice and rock" from the terminus. Claire Todd, a geology professor from Pacific Lutheran University, was on the Tahoma Creek suspension bridge as debris flows 2a and 2b moved down the watershed (Figure 4). When arriving at the bridge, she noted "a very high water/mud mark on [the] wall of [the] channel," quickly followed by a "loud roar

and terrific ground shaking" (Todd, 2015, personal communication). Continuing to observe the scene, she noted "a ~1.5 m boulder is exposed in the channel" as the flow passes, and within another minute, "roar and shaking resumes, a second flow passes, just as thick as the first—completely obscuring the large boulder again." Professor Todd witnessed the wave pass "exposing all of the large boulder again." Last, she recorded "a thin flow of hyperconcentrated water is passing … and a view upstream shows another low wave of hyperconcentrated flow approaching," noting that "these minor flows are not producing the roar or shaking that the first two offered."

The Emerald Ridge seismograph is located approximately 1 km (0.6 mi) from Tahoma Creek and accurately recorded the passage of each debris-flow surge. Using the seismic data as an input, after the event, we back-calculated the U.S. Geological Survey (USGS) Real-time Seismic Amplitude Measurement (RSAM) signature (Figure 4) (Endo and Murry, 1991). RSAM summarizes seismic activity for characterizing a volcano's changing seismicity in real time. We used it to down sample the seismic signal to an average amplitude over a set time, in this case, 30 seconds. The combination of the seismic data and RSAM calculations (Figure 4b) shows the passage of each debris-flow surge clearly.

One of the most interesting findings from the August 13 debris-flow sequence is the analysis of the soundscapes data in Figure 4c. The soundscapes monitor is a research effort by the National Park Service to understand the natural and unique soundscape of the park (National Park Service, 2018). Equipment emplaced along Tahoma Creek in 2015 fortuitously recorded the background noise in the months prior to and the day of the debris flow. The monitor recorded an anomalous decrease in river noise from the background level approximately 90 minutes before the arrival of the first debris-flow surge, which suggests creek blockage, filling of a temporary reservoir, and catastrophic failure as a debris flow. Each successive surge was recorded, and the river was relatively louder after the last debris-flow surge. This coincides with visual observations that the river was flowing much more vigorously after the event than before.

Park staff became aware of the debris-flow event at 12:02 PM when park volunteer Yonit Yogev called the MORA dispatch center on the radio and reported an outburst flood at Tahoma Creek trailhead. Yogev described the event as "telltale sounds of a rumbling train, a huge amount/sounds of trees, and a huge amount of water coming over the road out of the creek bed" (Yogev, 2015, personal communication; National Park Service, 2015). A park visitor, Zachary Jones, videoed the passing debris-flow surge (DF 3 in
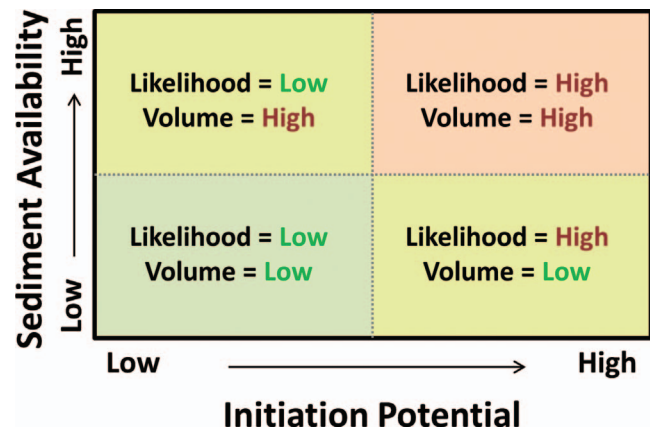
Figure 5. Simple matrix defining conceptual framework for debris-flow hazard mapping approach.

Figure 4) with his cellphone, which provided visual evidence of the flow.

Based on all observations and data observed from this event, we postulate that this event began as a physical blockage in the normal discharge of the glacier, perhaps as either a collapse of ice within the glacier or a small landslide just downstream of the glacier. This is evidenced by the anomalous and steady decrease in river noise from the soundscapes monitor just before 09:00 AM, showing that the total input to the river had dropped below the normal background level.

DEBRIS-FLOW HAZARD MAPPING

Mount Rainier's flanks and draining watersheds have varying geomorphic and watershed characteristics that, in turn, lead to varying patterns in potential for debris generation (Legg et al., 2014). Therefore, systematic mapping of relative hazards around MORA's flanks provides a critical tool in addressing the safety of park visitors as well as infrastructure management. The hazard mapping approach used here was based on a simple framework combining measures for debris-flow initiation potential and source sediment availability, with the basic idea that higher initiation potential leads to higher debris-flow likelihood, and higher sediment availability (abundance and proximity to drainage network) leads to greater debris-flow volume. This framework can be organized into a simple matrix showing varying combinations of debris-flow likelihood and volumetric potential as shown in Figure 5.

To assess debris-generating potential (likelihood), we made use of Legg et al.'s (2014) geomorphic characterization of debris-flow initiation points mapped after a major storm in November 2006. More specifically, the mapping approach presented in this current
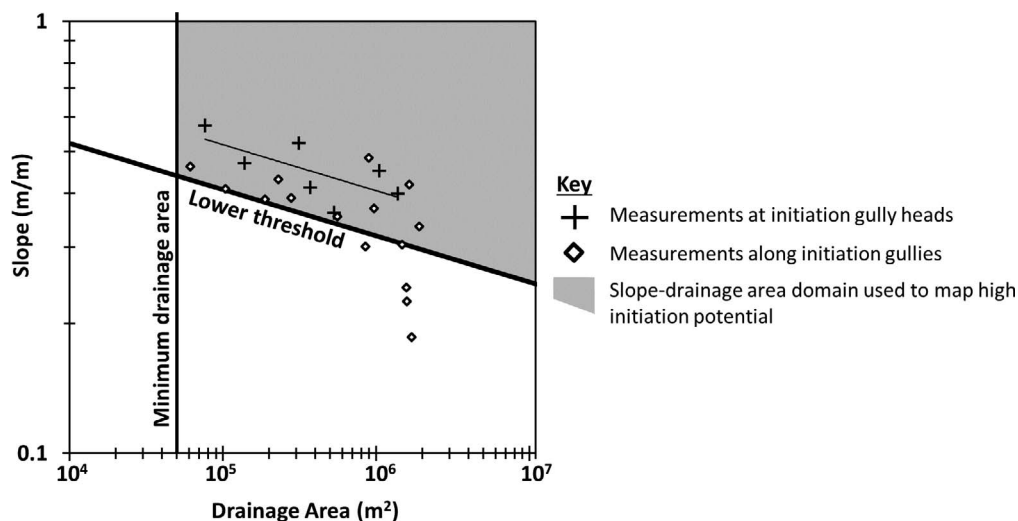
Figure 6. Plot of slope versus drainage area showing the slope–drainage area domain used to map gullies with high debris-flow initiation potential (based on data by Legg et al. [2014], who measured slope [*S*] and drainage area [*A*] within source gullies identified for the seven debris flows that initiated in the November 2006 storm). The lower domain bound visually bounds their sampled slopes and drainage area measurements and parallels their regression fit of gully head measurements (thin black line fit to crosses). The regression equation is $S = 1.769 \times A - 0.107$, and the lower threshold used for hazard mapping is $S = 1.40 \times A - 0.107$. A second domain boundary defines a minimum drainage area below which no debris-flow initiation points were mapped.

study made use of the gully slopes and drainage areas that Legg et al. (2014) measured at several initiation points of debris flows generated during a major storm in 2006. Based on their distribution of measured slopes and drainage areas of initiation points (Figure 6), we visually assigned slope and drainage area thresholds defining the domain of high debris-flow initiation potential (these thresholds are also shown in Figure 6). Using the slope–drainage area domain defined by our assigned thresholds, we then mapped high initiation potential segments of a drainage network across the full mountain, using a digitally generated drainage network generated from 1-m-spatial-resolution light detection and ranging (LiDAR) digital elevation models from 2009 (Figure 7).

Next, drainage network segments identified within the critical slope–drainage area domain were filtered and classified based on a qualitative assessment of sediment availability (addressing the second component of the Figure 5 conceptual matrix). Gullies initially identified using slope–drainage area mapping were filtered out from additional analysis if they occurred in forested settings (debris flows generated in forested settings are typically small relative to those originating from volcanic flanks), bedrock-dominated landscapes (high volcanic flanks above roughly 2,750 m [9,000 ft] above sea level are dominated by rockfall transport and show a general lack of surficial debris due to steep slopes [Czuba et al., 2012]), and glacier surfaces lacking supra-glacial debris (also with negligible sediment availability on the surface). The re-

maining gullies were then assigned a qualitative rating for relative sediment availability of "low," "medium," and "high," based on available surficial geologic maps (Crandell, 1969) and aerial photographs. In general, areas recently deglaciated and near glacier margins were assigned a high rating, areas near glacier margins with a mix of glacial debris and bedrock outcrops were assigned a moderate rating, and areas covered by older, more stable glacial debris (i.e., dating to the Last Glacial Maximum) and talus were assigned a low rating.

To assess and map variations in debris-flow hazard around the mountain, the mapping results (combining likelihood and sediment availability) were summarized on a watershed basis. The relative hazard rating incorporated a simple sum of drainage network lengths meeting the slope–drainage area criteria, weighted by sediment availability classified at each drainage network segment. The simple rationale for length is that watersheds with a greater length of gullies exceeding slope–drainage area thresholds in high-sediment settings are anticipated to have a higher likelihood of debris-flow production. Specifically, the lengths of network segments exceeding slope–drainage area thresholds and located within areas of "high" sediment availability were weighted 100 percent. Lengths of above-threshold segments with "medium" sediment availability were weighted at 50 percent. Low-sediment-availability segments were weighted at 0 percent (on the basis that these debris flows would be small and unlikely to impact infrastructure, even
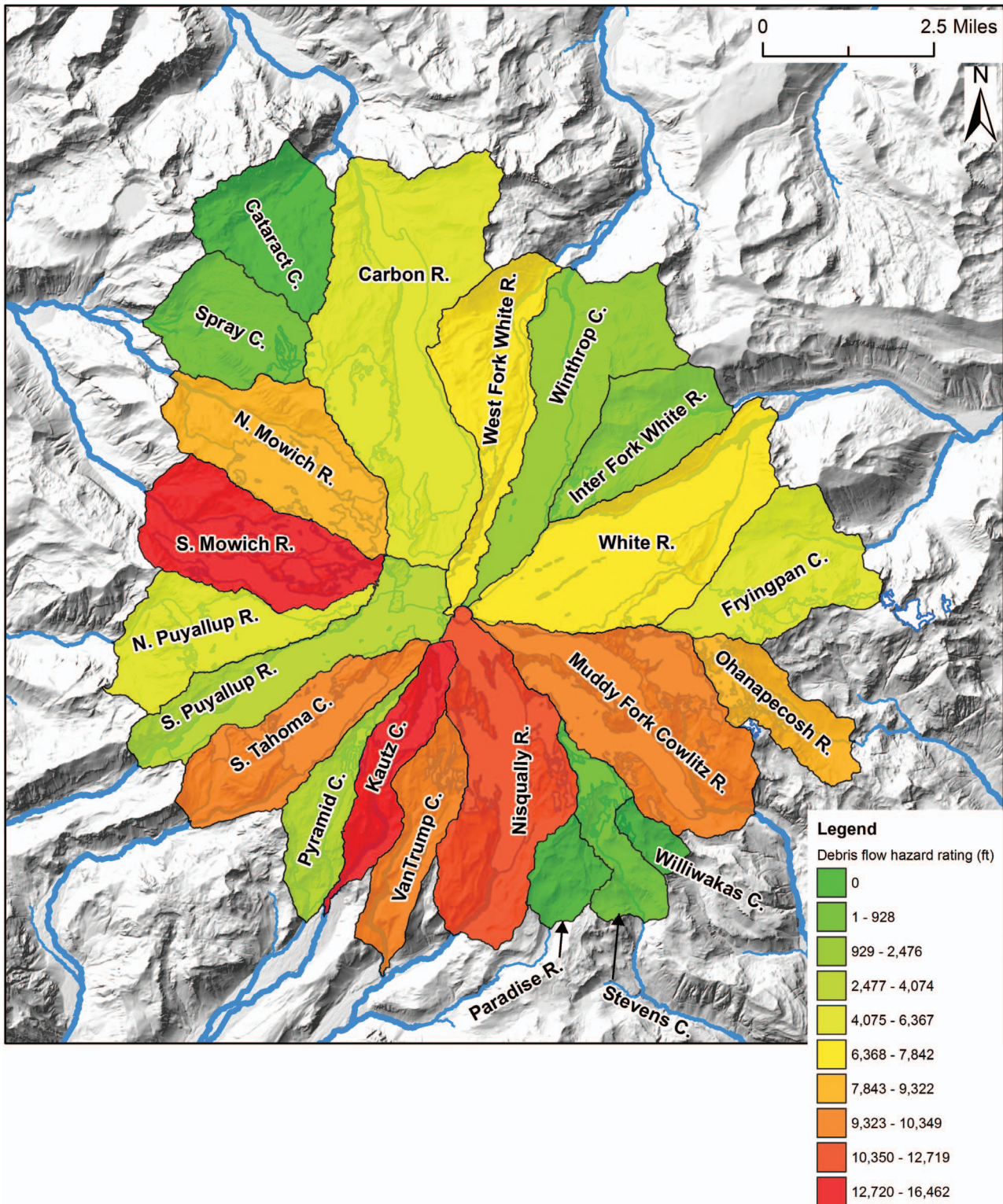
Figure 7. Map showing watersheds of major streams and rivers draining Mount Rainier and their debris-flow hazard ratings resulting from elevation distribution of high-hazard gullies mapped in the hazard assessment. High-hazard gullies are those with high initiation potential within mapped areas of high sediment availability. The indicated elevations were used to divide storm classes. The freezing level shown suggests that rain (as opposed to snow) is likely falling on approximately 95 percent of high-hazard gullies. The freezing level was calculated based on a measured temperature of 4.4°C (40°F) at the SNOTEL station and an assumed 5.5°C per vertical kilometer lapse rate. Weighted summation of high-hazard gullies was identified based on their slope, drainage area, and sediment availability. The density of hazard features within each designated watershed determined its hazard.

if initiated). The weighted sum of lengths resulted in a relative hazard rating to produce watershed-based hazard maps (incorporating both initiation potential and debris-flow volume) for the volcano, as shown in Figure 7. The watersheds with the 10 greatest hazard ratings, starting with the greatest, were the: (1) South Mowich River, (2) Kautz Creek, (3) Nisqually River, (4) Van Trump Creek, (5) Muddy Fork Cowlitz River, (6) South Tahoma Creek, (7) Ohanapecosh River, (8) North Mowich River, (9) White River (draining the Emmons Glacier), and (10) West Fork White River (draining the eastern margin of the Winthrop Glacier).

DEBRIS-FLOW HAZARD FORECASTING

The impetus for generating the debris-flow hazard forecast was to avoid having park staff and visitors in debris-flow-prone areas when events were likely to occur, like those conditions seen on August 13, 2015. The debris-flow hazard forecasting approach at MORA was based on two separate models combined, which incorporated different variables for dry, warm weather debris flows and cool, wet weather debris flows. The full model is shown in Appendix A.

Cool, Wet Weather Debris Flows

In recent decades, warm rainstorms occurring with low snowpack have been anecdotally associated with debris flows on MORA. These storm and debris-flow events typically occur in late fall, when atmospheric river storms bring intense tropical moisture from mid-latitudes and drop voluminous rain high on the volcanic flanks (Neiman et al., 2008). Prior to this study, there had been no systematic characterizations of debris-flow occurrence with respect to meteorological and antecedent hydrologic conditions. In practice, such a characterization could be paired with weather forecasts and *in situ* monitoring to forecast debris-flow hazards. This specific phase of our study focused on characterization of past storms and their associated debris-flow potential to develop a forecasting method for wet weather debris flows.

Debris-flow events recorded since 1980 were compiled from multiple sources and included in our analysis if (1) the debris flow's timing was known within a day, (2) it was associated with measurable precipitation, and (3) it occurred within the monitoring record of the snow telemetry (SNOTEL) station at Paradise (Natural Resources Conservation Service Site 679, elevation 1,640 m [5,381 ft]) on the southern flank of MORA. Debris-flow records included those from Walder and Driedger (1994a, 1994b, 1995), Driedger and Fountain (1989), and Copeland (2009). The SNO-
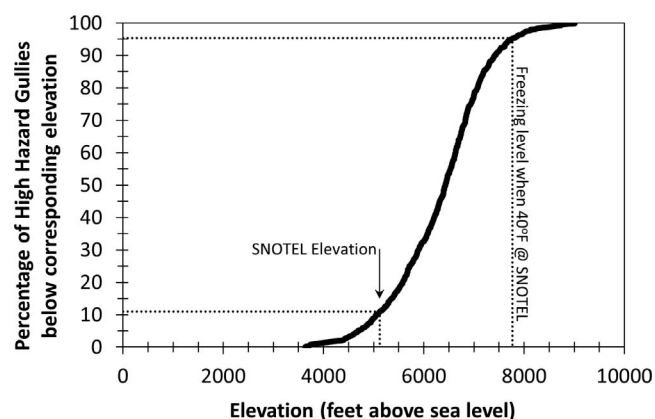

Figure 8. Elevation distribution of gullies mapped with high debris-flow hazard. High-hazard gullies are those with high initiation potential (based on slope and drainage areas) within mapped areas of high sediment availability. The indicated elevations and corresponding freezing levels were used as classification boundaries in the wet weather debris-flow forecasting method. Freezing levels were calculated based on recorded temperatures at the SNOTEL station and an assumed lapse rate of 5.5°C per vertical kilometer.

TEL station lies at the lower elevation range (see Figure 8) of high-hazard debris-flow gullies mapped in the effort discussed in the "Debris-Flow Hazard Mapping" section above. Data recorded at the station were therefore well suited for characterizing precipitation, temperature, and antecedent snowpack conditions within the elevation range of likely debris-flow initiation. For each debris-flow event, precipitation, temperature, and snowpack measurements were compiled for 1, 3, and 15 day periods on the day of and the day prior to the debris flow. These metrics were also compiled for all monthly maximum precipitation events for the full SNOTEL record to compare the known debris-flow-producing storms to the broader population of storms.

This data compilation effort resulted in a total of 11 debris-flow-producing storms that occurred between 1979 and 2014. All 11 storms had daily average temperatures (recorded at the SNOTEL station) above freezing, and all but two events had daily average temperatures above 4.4°C (40°F). Based on the elevation range of mapped high-hazard gullies (Figure 8) and an assumption of vertical lapse rates, these temperatures suggest that all storms were dropping rain (as opposed to snow) on a significant portion of the volcanic flanks most likely to initiate debris flows. A temperature of 4.4°C (40°F) at the SNOTEL, in particular, indicates temperatures above freezing for the full elevation band of high-hazard gullies, suggesting high potential for runoff generation in the zone of likely debris-flow initiation. All debris-flow-producing storms also had limited antecedent snowpack (only two exceeded 2.5 cm [1 in.] snow water equivalent (SWE) on the day of

the debris flow), therefore suggesting antecedent snowpack inhibits debris-flow generation. Potential mechanisms for this effect may include the ability of the snowpack to inhibit runoff generation and/or stabilize surficial colluvium. Additionally, there were negligible reductions in snowpack in the 3 days leading up to the 11 debris-flow events, suggesting snowmelt-derived runoff as an unlikely ingredient for debris-flow generation.

Precipitation quantities were further compared to an intensity-duration threshold for the nearby Seattle, WA, area developed by Chleborad et al. (2006), which was based on 3 day and 15 day cumulative precipitation totals in inches. The principals in play for this system are the assumptions that debris flows can be initiated by either heavy short-term storm inputs or longer-term saturation conditions, but also that both conditions can and often do occur in tandem. Initial comparisons to this landslide threshold found that eight of the 11 known debris-flow-producing storms exceeded the Seattle threshold; however, 247 of 376 monthly maximum storms (which had no recorded debris flows) from 1979 to 2014 also plotted above the threshold. The high number of non-debris-flow-producing storms plotting above the threshold suggests that it alone is a poor discriminator of debris-flow potential on MORA.

To explore potential refinements to the predictive model, we then filtered out monthly maximum storms from the analysis in a stepwise fashion based on their temperatures and antecedent snowpacks. The first step filtered out storms with greater than 12.7 cm (5 in.) SWE and/or 3 day average temperatures less than freezing. In the remaining group, 33 monthly maximum (non-debris-flow-producing) storms exceeded the Seattle threshold, in addition to the eight debris-flow-producing storms. These numbers indicate approximately 20 percent (8 of 41) of these storms (above-threshold storms with above-freezing temperatures and low snowpacks) generated debris flows. The next filter applied a temperature threshold of 4.4°C (40°F) instead of 0°C (32°F) and revealed that 5 of 14 storms (36 percent) exceeding the Seattle threshold produced debris flows. The increased proportion of debris-flow-producing storms indicates that warm temperatures (i.e., high freezing levels) are indeed a requirement for debris-flow generation. Overall, these results highlight the need for temperature and snowpack information to be coupled with precipitation thresholds in order to increase predictive capability of our wet debris-flow model.

The above analysis allowed us to develop a simple decision-tree approach to hazard classification as a planning tool for MORA (Legg, 2015). The approach uses 3 day precipitation and temperature forecasts in concert with measurements of SWE and 15 day precipitation totals to classify and forecast debris-flow hazards into low, medium, and high hazard categories over a coming 3 day period. More broadly, this effort represents an example of hazard forecasting in an alpine setting where seasonal temperature and snow fluctuations are major drivers of debris-flow potential.

Dry, Warm Weather Debris Flows

The method for forecasting dry weather debris flows is an expansion of Legg's (2015) model, which accounts for weather conditions that produce rapid glacier melt and potential for outburst floods that release and transform to debris flows. In total, 35 debris-flow events that occurred in a dry season (i.e., no rain and relatively warm temperatures, with average high temperature of approximately 18.3°C [65°F]) were compiled from the various sources mentioned in the previous section. From that list, antecedent weather information for the day of the event and the days leading up to the event itself was compiled from the Paradise SNOTEL station and other weather sources in the vicinity. A Monte Carlo analysis was completed on each weather variable to determine its relative importance to the overall detection of a debris flow. Once the relative weighting of each variable was completed, all days in the historic record were run through the model to determine the debris-flow hazard scores on those days (this included the wet weather debris flows) (Table 1).

The specific variables of interest for the dry side of the model were: (1) P_{18}, or 18 day precipitation total at Paradise, which was necessary to determine whether to run the dry side or wet side of the model; (2) T_{max}, which is the maximum daily temperature observed at Paradise; (3) $T_{max\ Percentile}$, which is the maximum temperature expressed as a percentile based on the historic maximum temperatures (1917–2017); (4) DS0SP, which is "days since zero snowpack," a relative variable used to determine when debris source areas will likely be snow-free; (5) $DD_{32\ 18}$, or the 18 day cumulative degree days above freezing; (6) P_3, or the 3 day precipitation total, a key dry weather variable defined by Walder and Driedger (1994a); and (7) SWE, or snow water equivalent. For the model, DS0SP was set as days since July 11th, which is the average "melt out" date at Paradise in the historic (1917–2017) record. The model uses known conditions to determine which type of condition is being predicted and therefore which equations to calculate. Each variable is then given a numeric score between 1 and 5 (see Appendix A), and the debris-flow hazard score is calculated (added) by the model.

Table 1. *Performance of current debris-flow hazard model based on all available weather data for the period of 1917–2017 at the Paradise SNOTEL station. Event type categories are split into known debris-flow and outburst flood days from the historic record. The undefined category means that weather conditions were not available to adequately calculate the debris-flow hazard score for that day. This table could not be assessed for relative effectiveness because all included counts are strictly historic events, and no modern events had yet occurred.*

Event Type	Model Type	Low	Medium	Medium High	High	Very High	Undefined
Debris flow (N = 42)	Wet	0	0	1	12	—	0
	Dry	3	4	6	11	5	0
	Total	3	4	7	23	5	0
Outburst flood (N = 8)	Wet	2	0	0	0	—	0
	Dry	3	1	0	1	1	0
	Total	5	1	0	1	1	0
Debris flow + outburst flood	Wet	2	0	1	12	—	0
(N = 50)	Dry	6	5	6	12	6	0
	Total	8	5	7	24	6	0
No debris flow or outburst	Wet	12,633	980	539	1083	—	942
flood (N = 31,647)	Dry	11,608	984	618	1001	540	719
	Total	24,241	1,964	1,157	2,084	540	1,661
Total, no. (%):		24,249 (76.50)	1,969 (6.21)	1,164 (3.67)	2,108 (6.65)	546 (1.72)	1,661 (5.24)

At this time, the method is still being refined as more data are uncovered about the antecedent weather conditions and as more debris flows occur in the park. Additionally, an improved Monte Carlo approach is being undertaken to improve the model. The performance of the model for all available dates between 1917 and 2017 is shown in Table 1. There have been only two debris-flow events since the system was designed and implemented, meaning that all other predictions of moderate to very high have been false positives. In general, those days with a debris flow or outburst flood from the historic record should have a higher score, whereas those days with no event should have a lower score for the model to be considered truly calibrated successfully.

Combination Forecast and Data Sources

The combination forecast (Appendix A) uses both the wet and dry sides to create a decision tree based on calculated weather factors. Weather information is downloaded every hour from the DarkSky.net Application Programming Interface (API). DarkSky provides a free ensemble forecast for individual locations throughout the park that is easily incorporated into the debris-flow hazard model. It should be noted that free access to this API is ending in 2021, and a new weather source is being sought for this model. Every 4 hours, these weather variables and antecedent weather observations are automatically compiled based on the wet or dry forecast and then run through the decision tree algorithm (Appendix A). A qualitative score (low, medium, medium high, high, or very high) is generated for the day of interest and the next 7 days. This is then reported on a website for monitoring and decision-based analysis by park staff. Hazard scores are tied to

weather forecasts and will change as forecasts are updated. While this process is automated, park staff still must monitor the model every day to determine the future relative risk for debris-flow activity.

REAL-TIME DEBRIS-FLOW MONITORING VIA RSAM SYSTEM

The final piece in the debris-flow hazard system at MORA is the ability to detect debris flows as they occur. As shown in the "Debris Flows in 2015" section, debris flows like those in 2015 have a seismic and RSAM signature that is distinctive. With assistance from the University of Washington's Pacific Northwest Seismic Network (UW PNSN), seismic data are run through the USGS RSAM program and binned into 30 second values. At 5 minute intervals, an automated computer script then downloads the RSAM values and runs through the data file looking for a "debris-flow-like signature." For the purposes of identification via the RSAM system, a debris-flow signature is roughly defined as an increasing signal above a set point over a set amount of time. If these values are exceeded, an alert is sent out to park staff for analysis and hazard notification via cellphone text messages and emails.

As an example, at the RER seismograph, the relevant variables are an RSAM value greater than 500 counts for over 5 minutes with an RSAM value that is increasing (slope > 0.030), on average, over those 5 minutes. Using this definition, three of the four debris flows on August 13, 2015 (2a/2b, 3, and 4), and an additional debris flow that occurred in Tahoma Creek on September 12, 2015 (not discussed in this paper), would have been detected with this system. Additionally, this system would have detected the second debris

flow on August 13th at roughly 10:20 AM, almost a full 2 hours before park staff were alerted to the event by witnessing it in person and reporting it on the radio. The goal would be to use this advance warning to notify park personnel and initiate emergency procedures, but the system had yet to be in effect prior to 2017 for an event that significantly impacts park infrastructure or use areas.

Real-time debris-flow monitoring via the RSAM system is currently being run on the RER seismograph (Puyallup, Tahoma, and South Tahoma Glaciers), Mt. Fremont (FMW) seismograph (Emmons, Inter, and Winthrop Glaciers), and Longmire (LO2/LON) seismograph (Kautz, Nisqually, Pyramid, Success, Van Trump, and Wilson Glaciers). Most of the major glacial streams at MORA now have some sort of seismic monitoring; those without, with the exception of Carbon Glacier, do not have extensive infrastructure development in their watershed boundaries.

The overall performance value of the RSAM system in detection of debris flows is being developed and has been improved by debris-flow events that occurred in 2019 (discussed in the next section). There have been several false-positive readings, almost exclusively due to wind noise (especially at RER). Local, regional, and teleseism earthquake events are such short-period and punctuated events that they are excluded in the analysis and rarely generate alerts. When false positives have been detected, staff are able to quickly analyze real-time seismic data to determine if the event is truly a debris flow or some other event. In this sense, the system is semi-automated and still requires human intervention in order to take the step from an alert generation to an alert being broadcast to the field. Last, we are not yet able to collocate exact drainages where a debris flow has occurred due to a paucity of seismic stations. However, a strong signal in one seismograph and relatively weak signals in others (as was the case in the August 2015 event) can help to determine a narrower geographic location for the event.

DEBRIS FLOWS IN 2019—MODEL CALIBRATION, VERIFICATION, AND VALIDATION, AND FUTURE WORK

A debris flow that occurred on August 5, 2019, in Tahoma Creek, between approximately 6:44 and 8:10 PM PDT (2019-08-06 01:44–03:10 UTC), provides validation information for the debris-flow forecasting and detection systems discussed here. Aerial reconnaissance on August 6 determined that the event originated from a sudden and significant change in the primary outlet stream from the terminus of the South Tahoma Glacier, which resulted in a surge of water within the

Figure 9. Terminus of South Tahoma Glacier on August 6, 2019, at approximately 2:48 PM PDT. The terminus is the darker band horizontally in the upper part of the photo. The outlet stream of the glacier had been on the left-hand side (river right) of the bedrock knob at the center of the photo and switched to the right side (river left) during the event, which incorporated loose, unstable ground moraine material and debris-covered stagnant ice downstream of the glacier and helped in debris-flow generation. (Photo: NPS/Scott Beason).

glacier incorporating a surfeit of sediment in proglacial areas downstream of the glacier (Figure 9). Four separate surges were observed in the RER seismograph, with each event lasting 20.8, 10.4, 15.1, and 39.1 minutes, respectively. The fourth surge had the strongest seismic signal, followed by the second, third, and first surge, respectively.

The qualitative debris-flow forecast for the 3 day period between August 4 and 6 was very high, high, and high, respectively. The forecast during this period was using the "dry" side of the algorithm and had inputs and outputs as shown in Table 2a. Unfortunately, the RSAM system did not detect any of the surges in this event; it nearly detected three of the surges, but critical exceedance thresholds were not met. In light of this, the critical threshold for debris-flow detection of RSAM counts from the RER system was re-calibrated from 500 to 400.

This calibration proved fortuitous in detecting a second debris-flow sequence about a month later on September 26, 2019. On this day, a single debris-flow sequence occurred between 5:46 and 5:59 PM PDT (2019-09-27 00:46–00:59 UTC). The now-calibrated debris-flow detection system detected the event at 5:49:15 PM PDT (00:49:15 UTC). During the day prior to the event and after this debris flow, numerous RSAM alerts were generated due to wind noise. Upon detection of this event (Figure 10), a field investigation was undertaken within an hour of the event itself, and in-field evidence indicated the presence of a

Table 2. *Input and output variables for debris-flow forecast day prior to, of, and after each of the August 5 and September 26, 2019, debris flows in Tahoma Creek. See Appendix A for model information and variable names.*

Date	T_{min} P_{15}	T_{avg} P_{18}	T_{max} SD	$T_{max perc}$ SWE	DS0SP T_A	DD_{32} T_B	$DD_{32\ 18}$ HS_{Dry}	P_1 Forecast Type	P_3 Score
(a) August 5, 2019, Tahoma Creek debris flow									
Aug 4	56.15	65.62	75.10	0.884	23	43	583	0.00	0.20
	0.03	0.23	0	0.00	False	False	110.0	Dry	VH
Aug 5	60.57	69.08	77.60	0.912	24	46	612	0.00	0.00
	0.21	0.21	0	0.00	False	False	60.0	Dry	H
Aug 6	62.23	70.16	78.10	0.936	25	46	637	0.00	0.00
	0.20	0.20	0	0.00	False	False	60.0	Dry	H
(b) September 26, 2019, Tahoma Creek debris flow									
Sep 25	37.55	46.06	54.58	0.433	75	23	309	0.00	0.44
	5.76	6.20	0	0.00	True	False	40.0	Wet	MH
Sep 26	41.36	44.94	48.52	0.268	76	17	308	0.73	0.82
	5.94	6.76	0	0.00	True	True	60.0	Wet	H
Sep 27	28.10	34.43	40.76	0.120	77	9	301	0.08	0.81
	4.99	5.80	0	0.00	True	False	52.5	Wet	M

SD = Snow Depth (inches), HS_{Dry} = Hazard Score for the Dry Side of the Model, VH = Very High, H = High and MH = Medium High

debris flow (new boulder levees, significant in-stream sediment motion, rapid water rise, rapid increase in turbidity, and a distinctive smell of sediment in the air). Viewing the raw seismic signal along with seismic spectra and RSAM information in a single plot is ex-tremely useful in visually excluding or including events as possible debris flows. Table 2b shows the forecast inputs and outputs for the event. It should be noted that the September event was using the "wet" side of the forecast algorithm and had the highest possible hazard
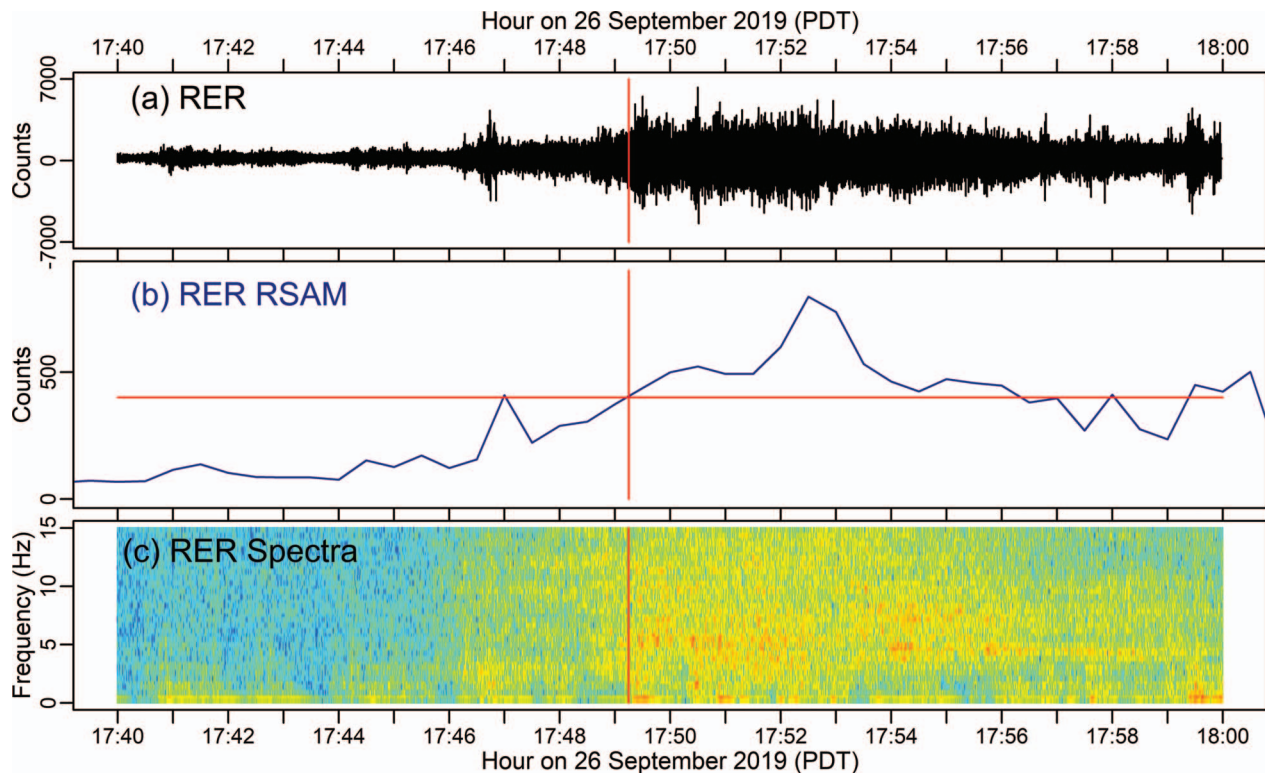

Figure 10. (a) Raw RER seismic trace, (b) RER RSAM signature, and (c) RER spectra of the September 26, 2019, debris-flow detection on the Emerald Ridge seismograph, including the time of detection of the event (vertical red line at 17:49:15 [5:49:15 PM] PDT; 00:49:15 UTC). Horizontal red line on RSAM plot (b) is the alert detection threshold (400 counts).

category. The September 26, 2019, debris-flow event was the first successful automated detection of a debris flow in the park.

It is interesting to note that the 2015 and 2019 events had a similar timing and pattern to the signal made by their debris-flow surges (i.e., an August event that had four surges and a September event that had a single surge). Both the debris-flow forecast and RSAM detection systems continue to be refined to improve the overall efficacy of the system. Additional debris-flow activity across the park, especially in those drainages that are monitored by the systems, will only improve the detection of debris flows over time. In-process proposals by the USGS to upgrade the seismic systems in the park, including the installation of infrasound sensors and additional seismometers, will only provide better data to help detect future debris-flow events.

CONCLUSIONS

Mount Rainier is an environment that is ideally suited for debris-flow genesis and has a rich history of these events. With our work, we have been successful in providing a forecast for debris-flow hazard based on antecedent weather conditions up to 7 days in advance of debris-flow days. We then can then detect individual debris flows using *in situ* seismometers and the RSAM system. As glaciers continue to retreat, new sediment sources will be exposed to annual storms and occasional outburst floods, all of which will contribute to the threat of debris flows in downstream areas. The forecasting and detection systems we have in place now are in their infancy and will be further refined as more events occur. Additional seismic installations planned in the next decade at MORA will only improve these systems and will provide better warning to park staff and visitors working and recreating at the park. Finally, the insights we are gaining in understanding debris-flow genesis and detecting debris flows at Mount Rainier could prove to be useful for similar efforts in analogous locales in the Pacific Northwest and across the world.

ACKNOWLEDGMENTS

REFERENCES

ANDERSON, C., 2015, personal communication, Mount Rainier National Park, 55210 238th Avenue E, Ashford, WA 98304.

BEASON, S. R., 2017, *Change in Glacial Extent at Mount Rainier National Park from 1896–2015*: National Park Service Natural Resource Report NPS/MORA/NRR—2017/1472, 98 p.

BEASON, S. R., 2012, *Small Glacial Outburst Flood Occurs on Mount Rainier—October 27, 2012*: Science Brief, National Park Service, Mount Rainier National Park, Ashford, WA, 3 p.

BULLOCK, A. B.; BACHER, K.; BAUM, J.; BICKLEY, T.; AND TAYLOR, L., 2007, *The Flood of 2006: 2007 Update*: Unpublished report, Mount Rainier National Park, Ashford, WA, 43 p.

CHLEBORAD, A. F.; BAUM, R. L.; AND GODT, J. W., 2006, *Rainfall Thresholds for Forecasting Landslides in Seattle, Washington, Area—Exceedances and Probability*: U.S. Geological Survey Open-File Report 2006-1064, 31 p. doi:10.3133/ofr20061064.

COPELAND, E. A., 2009, *Recent Periglacial Debris Flows from Mount Rainier, Washington*: Unpublished M.S. Thesis, Water Resources Engineering, Oregon State University, Corvallis, OR, 139 p.

CRANDELL, D. R., 1969, *Surficial Geology of Mount Rainier National Park, Washington*: U.S. Geological Survey Bulletin 1288, 41 p. doi:10.3133/b1288.

CRANDELL, D. R., 1971, *Postglacial lahars from Mount Rainier Volcano, Washington*: U.S. Geological Survey Professional Paper 677, 75 p. doi:10.313/pp677.

CZUBA, J. A.; MAGIRL, C. S.; CZUBA, C. R.; CURRAN, C. A.; JOHNSON, K. H.; OLSEN, T. D.; KIMBALL, H. K.; AND GISH, C. C., 2012, *Geomorphic Analysis of the River Response to Sedimentation Downstream of Mount Rainier, Washington*: U.S. Geological Survey Open-File Report 2012-1242, 134 p. doi:10.3133/ofr20121242.

DRIEDGER, C. L. AND FOUNTAIN, A. G., 1989, Glacier outburst floods at Mount Rainier, Washington State, U.S.A.: *Annals of Glaciology*, Vol. 13, pp. 51–55. doi:10.3189/S0260305500007631.

DRIEDGER, C. L. AND KENNARD, P. M., 1986, *Ice Volumes on Cascade Volcanoes: Mount Rainier, Mount Hood, Three Sisters, and Mount Shasta*: U.S. Geological Survey Professional Paper 1365, 38 p. doi:10.3133/pp1365

ENDO, E. T. AND MURRY, T. L., 1991, Real-time seismic amplitude measurement (RSAM): A volcano monitoring and prediction tool: *Bulletin of Volcanology*, Vol. 53, No. 7, pp. 533–545. doi:10.1007/BF00298154.

EWERT, J. W.; DIFENBACH, A. K.; AND RAMSEY, D. W., 2018, *2018 Update to the U.S. Geological Survey National Volcanic Threat Assessment*: U.S. Geological Survey Scientific Investigations Report 2018-5140, 40 p. doi:10.3133/sir20185140.

GEORGE, J. L. AND BEASON, S. R., 2017, Dramatic changes to glacial volume and extent since the late 19th century at Mount Rainier National Park, Washington, USA: *Geological Society of America Abstracts with Programs*, Vol. 49, No. 6, pp. 299694. doi:10.1130/abs/2017AM-299694.
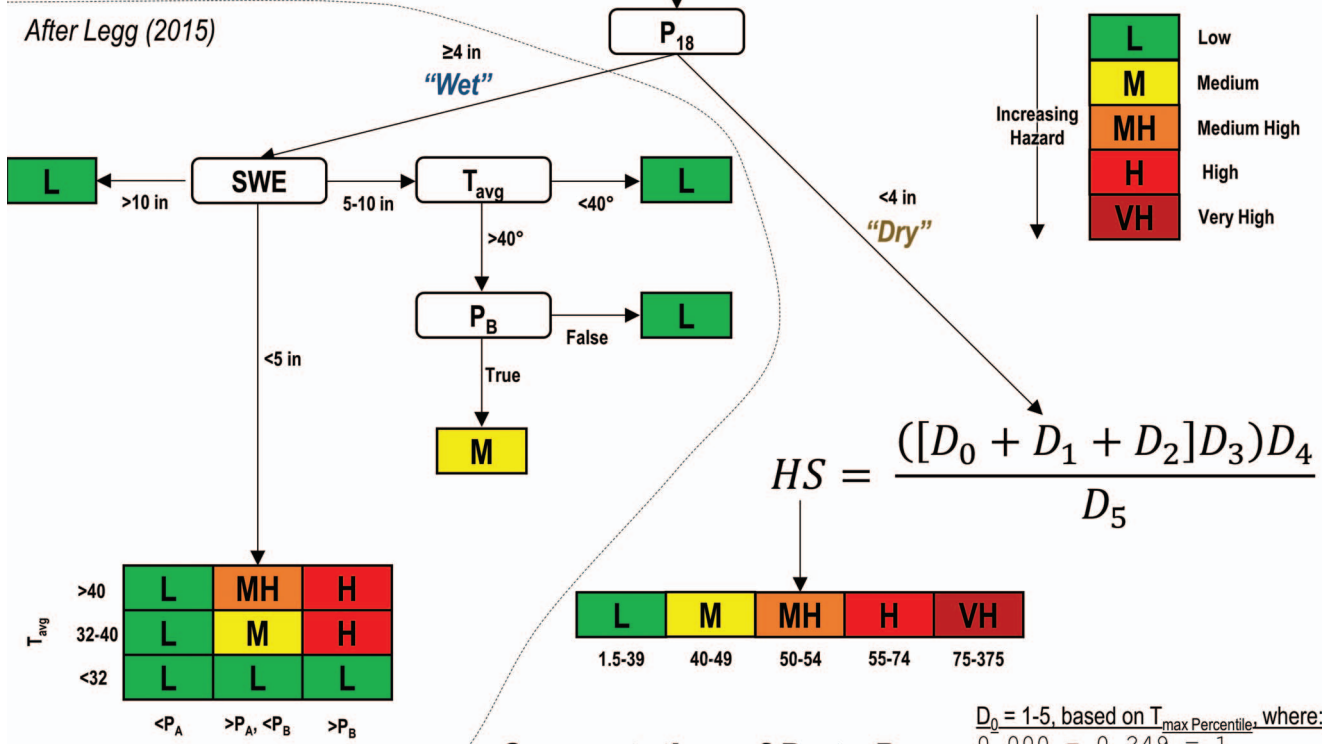
LEGG, N. T., 2015, *An Assessment of Hazards from Rain-Induced Debris Flows on Mount Rainier*: Unpublished internal document, Mount Rainier National Park, Ashford, WA, 30 p.

LEGG, N. T.; MEIGS, A. J.; GRANT, G. E.; AND KENNARD, P. M., 2014, Debris flow initiation in proglacial gullies on Mount Rainier, Washington: *Geomorphology*, Vol. 226, pp. 249–260. doi:10.1016/j.geomorph.2014.08.003.

LESCINSKY, D. T. AND T. W. SISSON, 1998, Ridge-forming, ice-bounded lava flows at Mount Rainier, Washington: *Geology*, Vol. 26, No. 4, pp. 351–354. doi:10.1130/0091-7613(1998)026<0351:RFIBLF>2.3.CO;2.

NATIONAL PARK SERVICE, 2018, *Mount Rainier Soundscapes*: Electronic document, available at https://www.nps.gov/mora/learn/nature/soundscapes.htm

NATIONAL PARK SERVICE, 2015, *NPS Dispatch Records for 13 August 2015*: Unpublished internal document, Mount Rainier National Park, Ashford, WA.

NEIMAN, P. J.; RALPH, F. M.; WICK, G. A.; KUO, Y. H.; WEE, T. K.; MA, Z.; TAYLOR, G. H.; AND DETTINGER, M. D., 2008, Diagnosis of an intense atmospheric river impacting the Pacific Northwest: Storm summary and offshore vertical structure observed with COSMIC satellite retrievals: *American Meteorological Society Monthly Weather Review*, Vol. 136, No. 11, pp. 4398–4420. doi:10.1175/2008MWR2550.1.

PIERSON, T. C. AND SCOTT, K. M., 1985, Downstream dilution of a lahar: Transition from debris flow to hyperconcentrated streamflow: *Water Resources Research*, Vol. 21, pp. 1511–1524. doi:10.1029/WR021i010p01511.

RICHARDSON, D., 1968, *Glacier Outburst Floods in the Pacific Northwest*: U.S. Geological Survey Professional Paper 600-D, pp. 79–86.

SAMORA, B. A. AND MALVER, A., 1996, *Inventory of Information on Glaciers in Mount Rainier National Park*: Unpublished report, Mount Rainier National Park, Ashford, WA, 417 p.

SCOTT, K. M.; VALLANCE, J. W.; AND PRINGLE, P. T., 1995, *Sedimentology, Behavior, and Hazards of Debris Flows at Mount Rainier, Washington*: U.S. Geological Survey Professional Paper 1547, 56 p. doi:10.3133/pp1547.

SISSON, T. W. AND VALLANCE, J. W., 2009, Frequent eruptions of Mount Rainier over the last ~2,600 years: *Bulletin of Volcanology*, Vol. 71, No. 6, p. 595–618. doi:10.1007/s00445-008-0245-7.

TODD, C., 2015, personal communication, Pacific Lutheran University, Department of Geosciences, Rieke Science Center, Room 158, Tacoma, WA 98447.

VALLANCE, J. W., 2005, Volcanic debris flows. In Jakob, M. and Hungr, O. (Editors), *Debris-Flow Hazards and Related Phenomena*: Springer Praxis Books, Springer, Berlin, pp. 247–274. doi:10.1007/b138657.

VALLANCE, J. W. AND SCOTT, K. M., 1997, The Osceola Mudflow from Mount Rainier: Sedimentology and hazard implications of a huge clay-rich debris flow: *Geological Society of America Bulletin*, Vol. 109, No. 2, pp. 143–163. doi:10.1130/0016-7606(1997)109<0143:TOMFMR>2.3.CO;2.

WALDER, J. S. AND DRIEDGER, C. L., 1994a, *Geomorphic Change Caused by Outburst Floods and Debris Flows at Mount Rainier, Washington, with Emphasis on Tahoma Creek Valley*: U.S. Geological Survey Water-Resources Investigations Report 93-4093, 100 p. doi:10.3133/wri934093.

WALDER, J. S. AND DRIEDGER, C. L., 1994b, Rapid geomorphic change caused by glacial outburst floods and debris flows along Tahoma Creek, Mount Rainier, Washington, U.S.A.: *Arctic and Alpine Research*, Vol. 26, No. 4, pp. 319–327. doi:10.2307/1551792.

WALDER, J. S. AND DRIEDGER, C. L., 1995, Frequent outburst floods from South Tahoma Glacier, Mount Rainier, U.S.A.: Relation to debris flows, meteorological origin and implications for subglacial hydrology: *Journal of Glaciology*, Vol. 41, No. 137, pp. 1–10. doi:10.3189/S0022143000017718.

YOGEV, Y., 2015, personal communication, Mount Rainier National Park, Ashford, WA 98304.

Daily Debris Flow Hazard

After Legg (2015)

P$_{18}$

≥4 in "Wet"

<4 in "Dry"

SWE

>10 in → L

5-10 in → T$_{avg}$

<40° → L

>40°

P$_B$

False → L

True

M

<5 in

Increasing Hazard		
L	Low	
M	Medium	
MH	Medium High	
H	High	
VH	Very High	

T$_{avg}$	<P$_A$	>P$_A$, <P$_B$	>P$_B$
>40	L	MH	H
32-40	L	M	H
<32	L	L	L

Forecasted Precip Threshold

$$HS = \frac{([D_0 + D_1 + D_2]D_3)D_4}{D_5}$$

L	M	MH	H	VH
1.5-39	40-49	50-54	55-74	75-375

Computation of D$_0$ to D$_5$:

D$_0$ = 1-5, based on T$_{max\ Percentile}$, where:
```
0.000 - 0.249 = 1
0.250 - 0.499 = 2
0.500 - 0.699 = 3
0.700 - 0.849 = 4
0.850 - 1.000 = 5
```

D$_3$ = 1-5, based on P$_3$, where:
```
0.00 - 0.09 = 1
0.10 - 0.49 = 2      (Walder and
0.50 - 0.99 = 3       Driedger,
1.00 - 1.50 = 4       1994)
     >1.50 = 5
```

D$_5$ = 1-2, based on T$_{max}$, where:
```
≥68 = 1
<68 = 2      (Walder and Driedger, 1994)
```

D$_1$ = 1-5, based on days since July 11, where:
```
-191 -    -1 = 1
   1 -    33 = 2     July 11 = average
  34 -    66 = 3     melt out date at
  67 -    99 = 4     Paradise between
 100 -   124 = 5     1917-2017
 125 -   139 = 4
 140 -   149 = 3
 150 -   159 = 2
 160 -   173 = 1
```

D$_2$ = 1-5, based on 18-day cumulative DD$_{32}$, where:
```
  0 - 199 = 1
200 - 399 = 2
400 - 499 = 3
500 - 599 = 4
    >600 = 5
```

D$_4$ = 1-5, based on SWE, where:
```
       >10.00 = 1
5.00 -  9.99 = 2
2.50 -  4.99 = 3
0.01 -  2.50 = 4
0.00         = 5
```

Variables:

DD$_{32}$ = Degree day above 32°F (dimensionless)
P$_A$ = Precipitation threshold A, P$_3$ = 2.5 − 0.67P$_{15}$
P$_B$ = Precipitation threshold B, P$_3$ = 4.5 − 0.67P$_{15}$
P$_3$ = 3-day (D1-D3) cumulative precipitation at Paradise (in)
P$_{15}$ = 15-day cumulative precipitation at Paradise prior to 3-day period (D4-D18) (in)

P$_{18}$ = 18-day cumulative precipitation at Paradise (in)
SWE = Snow water equivalent at Paradise (in)
T$_{avg}$ = Average temperature at Paradise (°F)
T$_{max}$ = Maximum temperature at Paradise (°F)
T$_{max\ Percentile}$ = Maximum temperature as a percentile compared to the historic temperature (1917-2017), (dimensionless)

Appendix A. Current debris-flow hazard forecast model in place at Mount Rainier.